Atmosphere **2015**, *6*, 1608-1632; doi:10.3390/atmos6111608

OPEN ACCESS

atmosphere

ISSN 2073-4433

www.mdpi.com/journal/atmosphere

Article

On the Importance of Aerosol Composition for Estimating Incoming Solar Radiation: Focus on the Western African Stations of Dakar and Niamey during the Dry Season

Mamadou Simina Drame [1,2,3,*], Xavier Ceamanos [1,4], Jean Louis Roujean [1], Aaron Boone [1], Jean Philippe Lafore [1], Dominique Carrer [1] and Olivier Geoffroy [1]

[1] Centre National de Recherches Météorologiques/Groupe d'etude de l'Atmosphère MEtéorologique (CNRM-GAME), UMR3589, Météo-France/Centre National de la Recherche Scientifique, Toulouse 31057, France; E-Mails: xavier.ceamanos@onera.fr (X.C.); jean-louis.roujean@meteo.fr (J.L.R.); aaron.a.boone@gmail.com (A.B.); jeanphilippe.lafore@meteo.fr (J.P.L.); dominique.carrer@meteo.fr (D.C.); olvr.geoffroy@gmail.com (O.G.)

[2] Département de Physique, FST, Université Cheikh Anta Diop de Dakar, Dakar BP 5085, Senegal

[3] Laboratoire de Physique de l'Atmosphère et de l'Océan Siméon Fongang, Dakar BP 5085, Senegal

[4] ONERA, The French Aerospace Lab, Toulouse 31055, France

* Author to whom correspondence should be addressed; E-Mail: mamadou.simina.drame@gmail.com; Tel.: +221-33-8259-364.

Academic Editors: Giovanni Pitari, Gabriele Curci and Robert W. Talbot

Received: 4 June 2015 / Accepted: 15 October 2015 / Published: 29 October 2015

Abstract: The article investigates the impact of aerosol composition on the estimation of the downwelling surface shortwave flux (DSSF). This initiative forms part of the efforts to improve the DSSF distributed by the Land Surface Analysis Satellite Application Facility (LSA-SAF). This operational product assumes invariant aerosol properties under clear sky conditions, which can be inaccurate for some regions of the world. This is the case of West Africa, where aerosol activity is not only highly variable due to frequent dust storms but also rich because of the coexistence of different aerosol species. This study was carried out over the West African stations of Dakar and Niamey, which represent different aerosol scenarios. Several dates during the dry season of 2006 were selected and classified into four different day types according to aerosol activity: *standard*, *clean*, *mixture* and *dusty* days. The diurnal evolution of DSSF and its direct and diffuse components were estimated for the selected dates by the current LSA-SAF algorithm and two other approaches using aerosol measurements from the Aerosol Robotic Network (AERONET) as input. The first

alternative approach took the diurnal evolution of the total aerosol optical depth (AOD) into account, assuming a default desert aerosol type. Experiments with this method showed a significant improvement in the estimated DSSF compared to the current LSA-SAF algorithm. For example, root mean square error (RMSE) improved from 170 W/m^2 to 50 W/m^2 for *dusty* days in Dakar and from 73 W/m^2 to 21 W/m^2 for *mixture* days in Niamey. This improvement resulted from the consideration of a time-varying AOD, which accounted for the rapidly changing aerosol load for these two day types. The second alternative approach tested included consideration of the diurnal variation of the aerosol load and composition. Again, this was done using AERONET data on the fine and coarse aerosol modes, which may be associated with different sized dust particles, sea salt, or soot from biomass burning (depending on the date). This enhanced consideration of the aerosol composition greatly improved the estimation of the diffuse component of the DSSF, further reducing the RMSE during *mixture* days from 50 W/m^2 to less than 10 W/m^2. This improvement mainly came from consideration of the right scattering properties of the aerosol particles, which may be significantly different for each aerosol type.

Keywords: solar radiation; aerosols; dust; West Africa; LSA-SAF

1. Introduction

West Africa is the world's largest source of mineral dust and biomass-burning particles [1]. Dust originating from this area represents 40% of global emissions of tropospheric aerosols [2]. Likewise, African fires result in about 40% of the total biomass-burning particles in the world [3]. These two types of atmospheric particles interact differently with incoming solar radiation, also called the downwelling surface shortwave flux (DSSF). While dust particles basically result in cooling of the surface by attenuation of direct radiation, biomass-burning particles contribute to surface warming by converting absorbed shortwave flux into longwave radiation re-emitted by these very particles towards the surface [4]. In West Africa, dust of natural origin predominates in the atmosphere throughout the year with abundance peaks between March and July [5]. Biomass-burning aerosols originating from anthropogenic activities [6] are mainly present during the dry season, between October and March [7]. Thus, both aerosol types may coexist in West Africa, resulting in aerosol optical depths (AOD) of 0.6 on average and up to 4 during strong dust storms [8].

The LSA-SAF (Land Surface Analysis Satellite Application Facility) program [9] distributes an instantaneous DSSF product every 30 min, which covers the Earth's disk as seen by the Meteosat Second Generation (MSG) satellite. Recently, this product has been found to contain seasonally dependent biases over African regions identified as significant aerosol sources [10–12]. These biases were detected during the pre-monsoon onset period (from May to June), when atmospheric dust concentration is at its peak (especially in March and June). For example, comparisons with ground observations taken during the African Monsoon Multi-disciplinary Analysis (AMMA) field campaign [13] revealed that the LSA-SAF DSSF product had been overestimated by approximately 10% (30 W/m^2) on average during June 2006 [12]. Ceamanos *et al.* showed in [14] that these biases mainly arose from

the assumption of constant aerosol properties (AOD and type) in the DSSF calculation. To reduce this bias, a new algorithm, referred to as SIRAMix (Surface Incident Radiation estimation using Aerosol Mixtures), was developed to compute DSSF, together with its direct and diffuse components, using dynamic aerosol properties and considering the coexistence of different aerosol types [14,15]. DSSF can be decomposed into direct and diffuse fluxes, which will be called "direct DSSF" and "diffuse DSSF" hereafter for the sake of simplicity. Likewise, the regular definition of DSSF (the sum of direct DSSF and diffuse DSSF) will be called "global DSSF". In [14], SIRAMix was tested successfully with aerosol data from the MACC-II (Monitoring Atmospheric Composition and Climate—Interim Implementation) project [16]. However, MACC-II data proved to be insufficiently accurate to enable a detailed investigation of the impact of aerosol composition on the estimation of direct and diffuse DSSF.

This article investigates the importance of considering not only the AOD but also the aerosol type (or composition) to estimate the different components of the DSSF in challenging conditions such as those found in West Africa. Two stations were selected, Dakar and Niamey, where aerosol activity is frequent and ground measurements of shortwave fluxes and atmospheric composition are available. The present work focuses on the dry months of 2006 in order to avoid clouds and to maximize the probability of encountering mixtures of biomass-burning and mineral dust aerosols. Experiments were conducted with the SIRAMix approach with the replacement of MACC-II aerosol data by more accurate AERONET (Aerosol Robotic Network) measurements as input. The use of accurate aerosol data is crucial to any study of the impact of aerosol composition on DSSF, as inaccurate AOD and aerosol composition may give rise to misleading conclusions. Two approaches were used to calculate global, direct, and diffuse DSSF. The first considered dynamic AOD and a fixed aerosol type. The second included the aerosol composition variations during the day. Improvements in global DSSF estimation obtained for each case were compared to results from the LSA-SAF product according to aerosol activity.

The article is organized as follows. Section 2 describes the characteristics of the ground stations, the selection of dates and their classification into day types according to aerosol activity. Section 3 describes the three approaches considered in this study for the estimation of surface fluxes and the associated inputs. The results of experiments are presented in Section 4. Finally, Section 5 summarizes the conclusions on the importance of the aerosol type in the estimation of incident shortwave radiation.

2. Case Study

2.1. Ground Stations and Period of Study

Two ground stations in West Africa were selected for the study: the Niamey site in Niger (13.48°N, 2.07°E) and the Dakar station in Senegal (16.95°W, 14.40°N). The study considered only the driest months of 2006 (*i.e.*, from January to early June and then from November to December) in order to avoid the presence of the clouds from the wet season. We recall that the present study only deals with clear sky (cloud-free) conditions. The dry season is characterized by mixtures of biomass-burning aerosols and mineral dust in the atmosphere [17] and sea salt aerosols are also found in coastal areas of West Africa such as Dakar throughout the year [18–20].

The Dakar and Niamey stations are equipped with instruments measuring a variety of parameters. For example, they are part of the AERONET network of sun photometers [21], which perform direct sun measurements every 15 min, with a 1.2° field of view at the nominal wavelengths of 440, 675,

870, 940, and 1020 nm. They provide accurate, real-time information on the (aerosol and gaseous) composition of the atmosphere, including AOD, aerosol size distribution, ozone and water vapor content and aerosol absorption and refractive indexes as described in [22]. In the work presented here, we used AERONET data corresponding to the cloud-screened and quality-checked level 2.0.

Measurements of global, direct, and diffuse DSSF are also available in Niamey from the Atmospheric Radiation Measurement (ARM) station [23]. A Radar-Lidar Mobile Facility (AMF) was also deployed at the Niamey station in 2006 as part of the AMMA field experiment [12,24]. The AMF is a portable facility equipped with cloud-dedicated instrumentation (vertically pointing 94-GHz radar and lidar) that provides continuous cloud profile documentation, radiosounding results, and surface budget measurements. The operations performed during the AMMA campaign [13] in Dakar provided similar flux measurements. The downward broadband shortwave radiative flux is measured in the spectral range of 200 to 3600 nm using a Kipp and Zonen CM22 pyranometer with a time step of 2 min. For diffuse radiation measurements, the direct solar radiation is intercepted by a 60 mm diameter sphere shadower tracking the Sun. The solar direct radiative flux, in the 200 to 4000 nm spectral range, is measured by a Kipp and Zonen CH1 pyrheliometer. These data were used differently in the present study. In particular, AERONET measurements served to account for aerosol activity for the surface flux estimation.

It is important to note that the AERONET station in Niamey was not operating between March and July 2006, and measurements from the AERONET station in Banizoumbou, Niger (13.32°N, 2.40°E), 50 km to the east, were used instead. This decision was based on two reasons. First, aerosols in this region tend to travel west from Banizoumbou to Niamey [8] and therefore aerosol activity in Niamey is very similar to that in Banizoumbou with a small time shift [25]. Second, experiments conducted over Niamey in the present study would help to evaluate the possibility of using low resolution aerosol data in the operational estimation of surface fluxes. For example, MACC-II data have a resolution of more than 100 km.

2.2. Selection of Dates and Classification into Day Types Based on Aerosol Activity

First, all clear sky (*i.e.*, cloud free) days in Dakar and Niamey during the driest months of 2006 were selected. This was done using the cloud information (C_{Ma}) acquired at these two stations (see Table 1). In Niamey, cloud masks are obtained from Radar and Lidar measurements [26]. The AERONET clear-sky detector (Level 2.0) is used for Dakar.

Table 1. Data used in the present study to select clear sky dates and to classify them into day types.

Parameter	Symbol	Use	Source
Ångström coefficient 440–870 nm	$\alpha_{440-870}$	Day type classification	AERONET
Aerosol optical depth at 550 nm	δ	Day type classification	AERONET
Cloud mask	C_{Ma}	Determination of clear sky days	Lidar + Radar or AERONET

Then all selected dates were classified into four day types: *clean*, *standard*, *dusty*, and *mixed* on the basis of aerosol activity. This classification is in agreement with the studies of [4,5], which used total AOD and Ångström coefficient. The Ångström coefficient provides information on the spectral evolution of the AOD and is calculated by the Ångström law on the basis of two AOD values at

different wavelengths. AERONET records of total AOD at 550 nm (δ) and Ångström coefficient from 440 nm to 870 nm ($\alpha_{440–870}$) [27] (see Table 1) were used to classify each clear sky date as follows:

- A day was classified as *clean* if the total AOD was less than or equal to 0.15, regardless of the value of the Ångström coefficient.
- A day was classified as *standard* if the AOD was between 0.2 and 0.5 and the Ångström coefficient was lower than 0.4. Statistically speaking, *standard* days represent the average and most frequent aerosol conditions in this region of Africa.
- A day was called *dusty* if the total AOD was beyond 0.5 and the Ångström coefficient was lower than 0.4. Fouquart *et al.* in [28] consider the latter value as the upper limit for mineral dust aerosols.
- A day was classified as *mixture* if the Ångström coefficient was greater than or equal to 0.4 and the AOD was greater than 0.15. The higher value of Ångström coefficient indicated the presence of fine particles in addition to the common middle-sized aerosols [29].

Table 2. Daily averaged Aerosol Robotic Network (AERONET) observations for each selected day (*clean*, *standard*, *mixture* or *dusty*) in Dakar (top table) and Niamey (bottom table). The parameters are total aerosol optical depth (AOD) (δ), coarse mode AOD (δ_c), fine mode AOD (δ_f), Ångström coefficient ($\alpha_{440–870}$), and single scattering albedo (SSA), all at 550 nm except the Ångström coefficient. For the "Date" line, the first line corresponds to the year, the second to the month, and the third to the day number.

DAKAR

Day Type			***Clean***				***Standard***					***Mixture***						***Dusty***		
	06	06	06	06	06	06	06	06	06	06	06	06	06	06	06	06	06	06	06	06
Date	02	02	02	02	03	02	02	03	03	04	01	02	02	02	05	03	03	03	03	04
	16	22	25	28	01	23	24	15	31	01	21	01	03	04	03	10	11	12	13	05
δ	0.12	0.10	0.15	0.13	0.09	0.19	0.23	0.51	0.50	0.45	0.91	0.25	0.42	0.30	0.44	1.93	2.46	1.69	0.91	0.73
δ_c	0.07	0.06	0.10	0.07	0.06	0.11	0.13	0.35	0.33	0.32	0.26	0.08	0.11	0.08	0.09	1.41	1.62	1.24	0.66	0.52
δ_f	0.05	0.04	0.05	0.06	0.03	0.08	0.10	0.16	0.17	0.13	0.65	0.17	0.31	0.22	0.35	0.52	0.84	0.45	0.25	0.21
$\alpha_{440–870}$	0.38	0.30	0.13	0.41	0.27	0.57	0.38	0.15	0.20	0.15	0.85	0.86	0.91	0.92	1.14	0.11	0.12	0.10	0.12	0.16
SSA	0.91	0.88	0.93	0.87	0.90	0.89	0.89	0.92	0.92	0.92	0.83	0.80	0.85	0.82	0.88	0.94	0.95	0.95	0.94	0.94

NIAMEY

Day Type			***Clean***				***Standard***					***Mixture***						***Dusty***		
	06	06	06	06	06	06	06	06	06	06	06	06	06	06	06	06	06	06	06	06
Date	01	02	11	11	11	02	02	04	04	05	01	01	01	01	12	03	03	03	04	06
	16	25	05	25	26	04	06	06	29	23	01	09	11	22	15	10	12	21	19	13
δ	0.13	0.14	0.09	0.06	0.08	0.27	0.32	0.22	0.27	0.57	0.32	0.44	0.34	0.34	0.27	1.54	0.83	1.01	1.68	1.50
δ_c	0.03	0.08	0.05	0.02	0.04	0.15	0.20	0.14	0.17	0.20	0.09	0.09	0.08	0.08	0.12	0.99	0.55	0.64	1.07	1.04
δ_f	0.10	0.06	0.04	0.04	0.04	0.12	0.12	0.08	0.09	0.37	0.23	0.35	0.26	0.26	0.15	0.55	0.28	0.37	0.61	0.46
$\alpha_{440–870}$	0.92	0.47	0.49	0.73	0.52	0.40	0.37	0.27	0.21	0.14	1.01	1.12	0.99	1.04	0.66	0.16	0.19	0.20	0.19	0.16
SSA	0.79	0.87	0.86	0.92	0.92	0.88	0.91	0.92	0.90	0.95	0.80	0.84	0.78	0.80	0.88	0.96	0.95	0.94	0.97	0.95

According to the classification above, there were 9% of *clean* days, 40% of *standard* days, 31% of *mixture* days and 20% of *dusty* days in Dakar during the clear-sky days of 2006. Similar proportions were found in Niamey with the following values: 9% *clean*, 40% *standard*, 28% *mixture* and 23% *dusty*. Generally, *clean* days occur between October and early March, *mixture* days during winter (November-February), and *dusty* days from March to October.

For the experiments reported in the present article, we selected the five dates that were the most representative of each day type. Table 2 shows the daily averaged total AOD (δ) and the Ångström coefficient ($\alpha_{440-870}$) for the total of 20 selected days (5 days per day type) for the two stations in this study. Additional parameters—coarse mode AOD (δ_c), fine mode AOD (δ_f), and single scattering albedo (SSA)—will also be used in the following sections.

3. Estimation of Surface Fluxes

3.1. Experimental Design

The experiments were conducted for the 20 selected dates (five dates per day type). For each day and station, the diurnal evolution of the global DSSF was calculated using three methods. The first one was the approach corresponding to the operational LSA-SAF global DSSF product. Ground measurements were used as input. The second and third approaches (SIRAMix1 and SIRAMix2) were based on the SIRAMix methodology [14], which allows the direct and diffuse surface fluxes forming the global DSSF to be calculated by using aerosol properties as input. Under clear sky conditions, aerosols are the major cause of the scattering in the atmosphere that results in the splitting of global DSSF into its direct and diffuse components. The SIRAMix1 approach uses the total AOD provided by AERONET at each instant of time and considers a fixed desert-type aerosol model. The SIRAMix2 approach considers not only the AOD given by AERONET but also the aerosol composition. This is done by modeling the aerosol layer as the combination of the extinction properties of the two predominant aerosol types. More details on the three methods are given in Section 3.3.

3.2. Data Base of Aerosol Properties

A database of aerosol optical properties was used for the SIRAMix1 and SIRAMix2 approaches. These data were necessary to accurately simulate incoming solar radiation. Several data bases [30–33], each containing the optical properties of a given aerosol layer have been proposed in recent decades. The calculation of aerosol radiative properties is quite challenging since different aerosol types are related to distinct optical properties [29] and the properties of aerosol mixtures are generally poorly documented. This is particularly the case for the combination of mineral dust, biomass burning and sea salt found in West Africa [4].

The present work used the OPAC (Optical Properties of Aerosols and Clouds) package, which provides optical properties for 10 elementary aerosol components [33]. In OPAC, these components are combined in different ways to form ten aerosol types representing default atmospheric conditions across the world. While uncertainties are known to exist in OPAC—especially for the less known dust and soot particles—the studies in [29,34,35] affirm that OPAC is one of the best data bases determining single-scattering properties of spherical aerosols for broadband radiative calculations. Furthermore, OPAC can be conveniently combined with radiative codes such as libRadtran [36] to simulate shortwave aerosol quantities. Different data from OPAC were used for the second (SIRAMix1) and third (SIRAMix2) approaches.

3.2.1. OPAC Desert Aerosol Model

The SIRAMix1 approach estimated global, direct and diffuse DSSF by using SIRAMix with the OPAC default aerosol model referred to as desert. This aerosol type is claimed to be representative of the optical properties of aerosols over most of the desert areas in the world. The OPAC desert type combines three predominant modes of mineral dust particles: the MIneral Nuclei Mode (MINM, for small particles), the MIneral Accumulation Mode (MIAM, for medium-sized particles), and the MIneral Coarse Mode (MICM, for coarse particles). Table 3 shows the single scattering albedo (SSA) at 500 nm and the mode radius [33] in the dry state corresponding to these three dust components.

Table 3. Microphysical properties of some OPAC (Optical Properties of Aerosols and Clouds) aerosol components in the dry state. Single scattering albedo (SSA at 500 nm) and mode radius were retrieved from [32,33].

	MINM	MIAM	MICM	SSAM	SOOT
SSA	0.95	0.83	0.62	1.00	0.23
Mode radius (μm)	0.07	0.39	1.90	0.209	0.0118

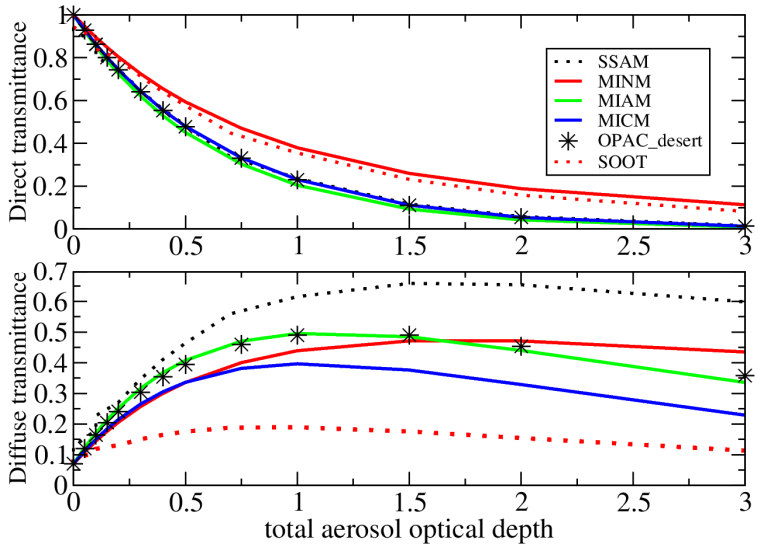

Figure 1. Direct (**top**) and diffuse (**bottom**) transmittance for the OPAC aerosol components used in this article (MIneral Nuclei Mode (MINM), MIneral Accumulation Mode (MIAM), MIneral Coarse Mode (MICM), Sea Salt Accumulation Mode (SSAM) and soot component (SOOT)) and the desert aerosol type (OPAC_desert is a combination of MINM, MIAM and MICM). A solar zenith angle of 50° was set to calculate all transmittances, as it corresponds to the average value in West Africa during the dry season.

The shortwave direct and diffuse transmittances of the OPAC desert type are shown in Figure 1. It can be seen that the desert aerosol type is dominated by the medium-sized particle component (MIAM), as the two transmittances are very close to each other. Also, it is important to note the different trends that may be observed for diffuse transmittances with an AOD of 1 and beyond. While diffuse transmittance starts to decrease for MIAM, MICM and the desert model, it continues to increase for the less-absorbing fine dust mode, MINM. These differences may be important when

using the desert aerosol type under an enhanced presence of fine dust particles. This particularity may help to explain why some studies show the OPAC desert type to be more absorbing than is observed *in situ* or by satellite for North African regions [37–41].

3.2.2. OPAC Elementary Aerosol Components

The SIRAMix2 approach used SIRAMix with two OPAC aerosol components that were different for each selected date. In addition to the dust components MINM, MIAM, and MICM described above, the present study also considered the Sea Salt Accumulation Mode (SSAM) and the soot component (SOOT). SSAM accounts for medium-sized sea salt particles found over the coastal regions of West Africa. Sea salt aerosols are often characterized by a low AOD compared to other aerosols [29] and a low absorption (SSA > 0.97). SOOT represents biomass-burning aerosols from fires occurring in West Africa during the dry season. Soot particles (or black carbon) are highly absorbing—SSA = 0.23 at 500 nm (see Figure 1)—and are often mixed with other components such as desert dust [42,43]. Also in Figure 1, we see the strong contrast between the low absorption of SSAM and the absorption of SOOT, which is the highest of all OPAC aerosol components. It is important to note that spherical particles are assumed for all OPAC aerosol components.

3.3. Methods for Estimation of Surface Fluxes

The three approaches for simulating the different DSSF terms consider aerosol conditions with different levels of detail.

The operational LSA-SAF approach: Geiger *et al.*'s estimation [44] of the global DSSF uses a physically-based parameterization considering a simplified plane-parallel atmosphere with constant pressure. Under clear sky conditions, incoming solar radiation is considered to be scattered by aerosols and gas molecules, and absorbed by water vapor, ozone, aerosols, and, to a lesser extent, oxygen and carbon dioxide. Aerosol conditions are considered to be constant, with a typical continental aerosol type and a surface visibility of 20 km (AOD of 0.25 at 550 nm, approximately).

The recent SIRAMix approach developed by Ceamanos *et al.* in [14] was used as the keystone of the second and third methods. The advanced physical parameterization (analytical formulae) employed in this method allows it to retrieve the direct and diffuse DSSF through the use of time-evolving aerosol properties (load and type) as input. The global DSSF is obtained by simply adding the two surface fluxes. Multiple values of aerosol transmittances and albedo are pre-computed using the radiative transfer code libRadtran for several default aerosol components and types, and are stored in a look up table (LUT). The LUT is accessed for each direct or diffuse DSSF calculation in order to obtain the aerosol radiative quantities corresponding to each instant of time. We refer the reader to the Appendix for more details about the SIRAMix approach. Two configurations of SIRAMix regarding the definition of the aerosol layer were used in the present work.

The SIRAMix approach with a desert aerosol model (SIRAMix1): In this configuration, SIRAMix took the variations of the aerosol load with time into account by using AERONET instantaneous measurements of total AOD as input. However, SIRAMix1 considered a fixed aerosol type to calculate the LUT: the OPAC desert aerosol model. Hence, the aerosol size distribution was assumed to be mono-modal, considering only the predominant type of particles.

The SIRAMix approach with two predominant aerosol components (SIRAMix2): The second configuration of SIRAMix estimated the direct and diffuse DSSF, considering the two predominant aerosol components at each instant of time. The aerosol size distribution was therefore assumed to be bimodal with one mode made by fine aerosol particles and the other made by coarse particles (Dubovik and King in [22] defined the particle radius separating fine and coarse modes as 0.6 μm). The bimodal distribution is accepted as the most appropriate model for aerosols by many studies [29,30,45]. In fact, practically all AERONET observed size distributions have a bimodal structure, especially in Africa [42]. AERONET stations provided the AOD corresponding to the fine and coarse aerosol modes.

The above data were used as input to SIRAMix, in which each aerosol mode is associated with a single aerosol component from OPAC (MINM, MIAM, MICM, SOOT, or SSAM, see Section 3.2.2). This flexibility satisfies the situation when the predominant dust particles are not smaller than a micron (MINM and MIAM) but larger (MICM). This is the case of some African regions near the dust sources [46]. In SIRAMix2, the two predominant aerosol species were determined each day using ancillary data, as explained in Section 3.5. The pair of pre-computed LUTs, one for each predominant aerosol component, provided the individual transmittances and albedo that were combined to calculate the radiative properties of the two-component aerosol layer. This combination was performed following the approach in [15] (see Equation (A11) in Appendix), which is also used by SIRAMix in [14] with five aerosol species.

3.4. Inputs for Estimation of Surface Fluxes

Table 4 lists the data sets used as input for the methods LSA-SAF, SIRAMix1, and SIRAMix2.

Table 4. Data used in the present study for the Land Surface Analysis Satellite Application Facility (LSA-SAF), SIRAMix1, and SIRAMix2 methods. All inputs come from *in situ* observations from AERONET except for the surface albedo, which corresponds to the satellite product released by the LSA-SAF project.

Parameter	Symbol	Used in Methods	Source
Solar zenith angle	θ_0	LSA-SAF, SIRAMix1, SIRAMix2	AERONET
Precipitable water in cm^{-1}	u_{H2O}	LSA-SAF, SIRAMix1, SIRAMix2	AERONET
Total ozone column in Dobson units	u_{O3}	LSA-SAF, SIRAMix1, SIRAMix2	AERONET
Surface albedo	α	LSA-SAF, SIRAMix1, SIRAMix2	LSA-SAF
Aerosol optical depth at 550 nm	δ	SIRAMix1	AERONET
Coarse mode AOD at 550 nm	δ_c	SIRAMix2	AERONET
Fine mode AOD at 550 nm	δ_f	SIRAMix2	AERONET

Note that all inputs came from ground measurements except for the surface albedo, which corresponded to the satellite product disseminated by the LSA-SAF project [47]. While the solar

zenith angle (θ_0), precipitable water (u_{H2O}), total ozone column (u_{O3}), and surface albedo (α) were used for all methods, only the SIRAMix-based methods, SIRAMix1 and SIRAMix2, used aerosol data as input. In particular, SIRAMix1 used AERONET measurements of total AOD at 550 nm (δ) to set the diurnal variations of aerosol loading, whereas SIRAMix2 used the coarse mode AOD (δ_c) and fine mode AOD (δ_f), both at 550 nm, to set the aerosol load for each predominant aerosol type.

3.5. Determination of Predominant Aerosol Types for Each Selected Day

To run the SIRAMix2 approach, the two predominant aerosol components for each date and station must be known. This information was determined on the basis of the following data (see Table 5).

Table 5. Data used in the present study for the determination of predominant aerosol types.

Parameter	Symbol	Source
Back-trajectories	-	NOAA HYSPLIT
Spectral aerosol single scattering albedo	$\omega_0(\lambda)$	AERONET
Aerosol size distribution of the particle volume in SIRAMix2	dV(r)/dlnr	AERONET
Lidar	-	Dakar

AERONET size distribution data allowed the average particle size of the existing modes to be identified. Also, the AERONET-derived single scattering albedo (SSA) of the aerosol particles provided information on the absorption properties. Figures 2 and 3 show the daily-averaged aerosol size distribution and the spectral signature of SSA measured by AERONET for each date, in Dakar and Niamey respectively.

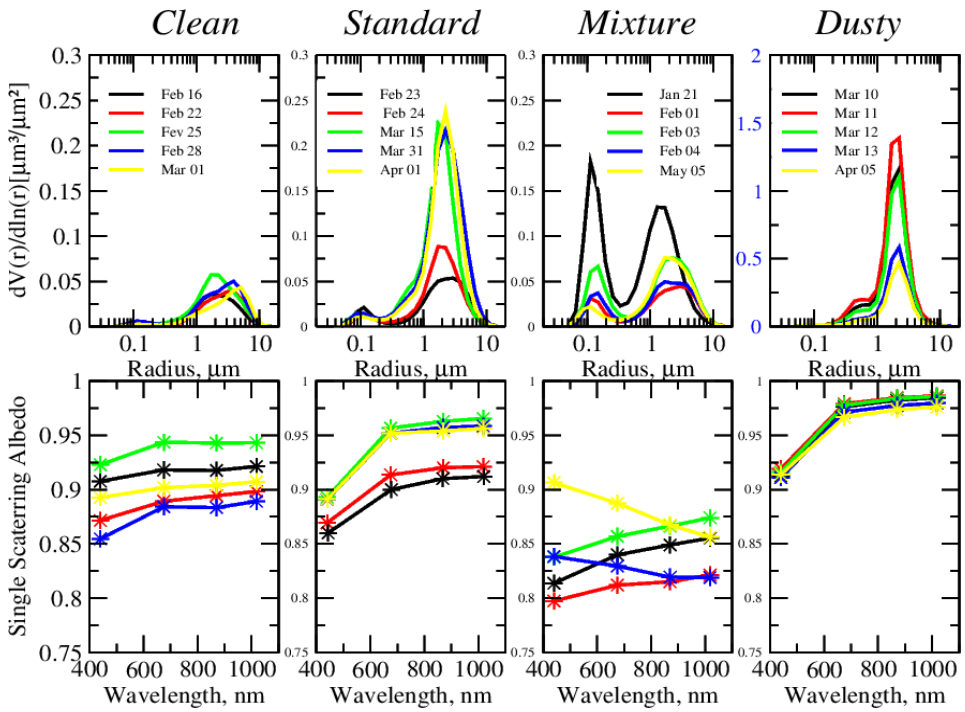

Figure 2. (**top**) Aerosol size distribution and (**bottom**) single scattering albedo retrieved by the AERONET station in Dakar for the five days selected for each day type (*clean*, *standard*, *mixture* and *dusty*). Note that the scale of the vertical distribution is different for *dusty* days (in blue).

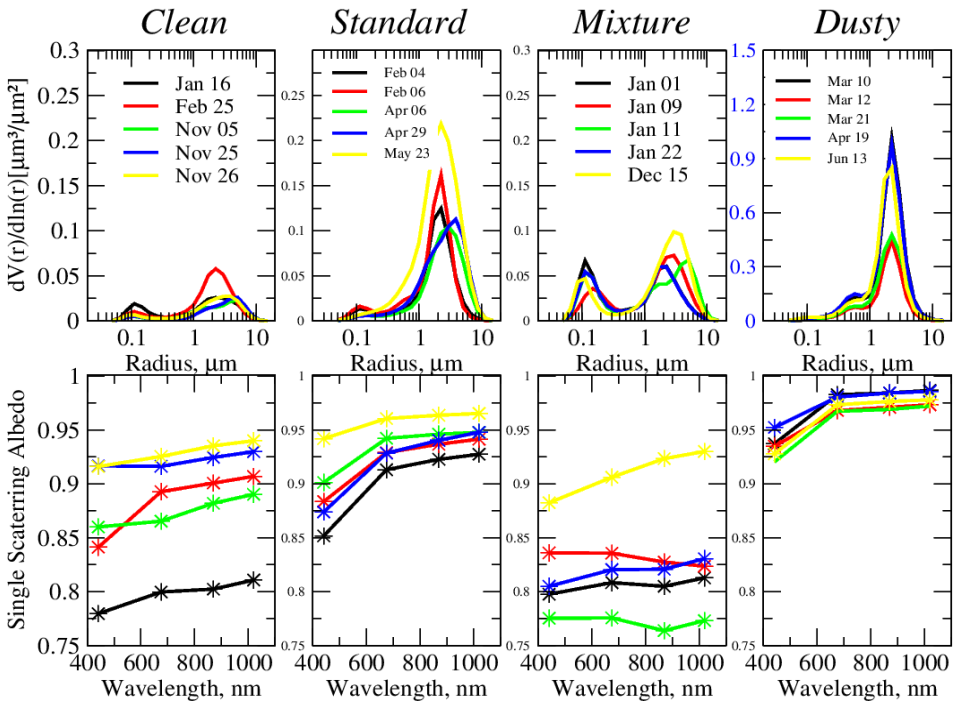

Figure 3. Same as Figure 2 for Niamey.

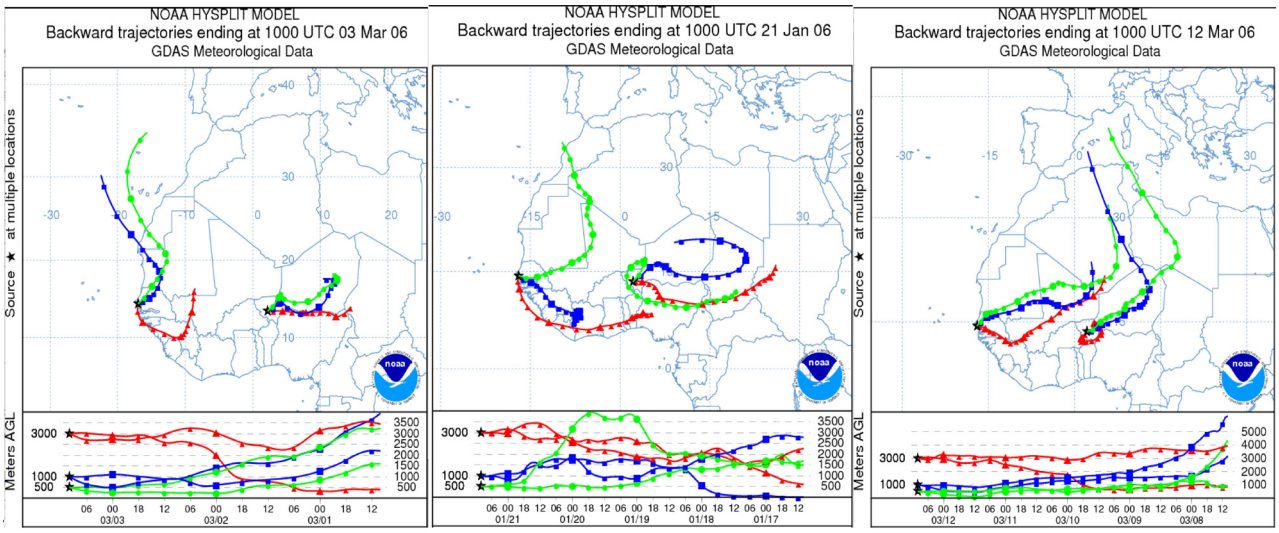

Figure 4. Backward trajectories traced by the NOAA Hybrid Single Particle Lagrangian Integrated Trajectory (HYSPLIT) model with endpoints in Dakar (black star on the coast) and Niamey (black star inland) for 12:00 UTC on the following days in 2006: (**left**) *clean* day 3 March; (**center**) *mixture* day 21 January and (**right**) *dusty* day 11 March. The time step is 6 h for 120 h (5 days). At the bottom of each map, back trajectories are represented for the following atmospheric heights: 500 m (green), 1000 m (blue) and 3000 m (red). These curves represent the height of the air mass during particle transport.

Air mass back trajectories from the Hybrid Single Particle Lagrangian Integrated Trajectory (HYSPLIT) model [48] were also used to identify the geographical source of aerosol particles. HYSPLIT trajectories were calculated at different altitudes of the atmosphere in order to identify the location of multiple aerosol sources. Figure 4 shows the computed air mass backward trajectories at

altitudes of 0.5 km (green lines), 1 km (blue lines), and 3 km (red lines). These altitudes were selected according to Lidar measurements made in Dakar [4,49] showing that aerosol particles are located between 1 and 2 km (medium-sized or coarse particles, mainly) and between 3 and 4 km (fine particles, likely). This Lidar system is a 532 nm micropulse backscattering LIDAR. In Figure 4, HYSPLIT back trajectories with end points in Dakar and Niamey are plotted for the following dates in 2006 at 10:00 UTC: (left) 3 March (*clean* day), (middle) 12 March (*dusty* day), and (right) 21 January (*mixture* day). Trajectories corresponding to other dates were found to be similar.

3.5.1. Aerosol Characterization for *Clean* Days

Figure 4 (left) provides evidence that particles arriving at Dakar at heights of up to 2 km on the *clean* day of 3 March came from the Atlantic Ocean while particles at heights of 3 km and beyond originated in desert areas. This indicates a possible mixture of sea salt and dust aerosols, as suggested in [50]. The Lidar sensor in Dakar showed a peak of aerosol particles located between 0 and 2 km for 3 March [4], pointing to the presence of sea salt particles fo*r clean* days in Dakar. Backward trajectories in Figure 4 (left) for *clean* days in Niamey point to Northern Niger, which is a known source of mineral particles. The spectral signature of the SSA for *clean* days is quite similar to Dakar's except for a generally lower value indicating a stronger absorption. This fact may be explained by the presence of fine black carbon particles coming from fires in the Nigeria region (see Figure 4), which is confirmed by the relatively high Ångström coefficient ($\alpha_{440-870}$ between 0.45 and 0.92, see Table 2).

In conclusion, the SIRAMix2 approach for *clean* days in Dakar and Niamey used the OPAC component MIAM for the coarse mode. The fine mode was modeled by SSAM for Dakar and SOOT for Niamey.

3.5.2. Aerosol Characterization for *Standard* Days

Standard days were characterized by a maximum of coarse mode particles, with values of size distribution around 0.25 $\mu m^3/\mu m^2$. Table 2 shows that the fine mode AOD (δ_f) was generally less important than the coarse mode AOD. Both stations had a very similar SSA spectral signature, which was characteristic of mineral particles, the increase of absorption for shorter wavelengths being due to the presence of iron oxides in mineral dust [4].

In conclusion, for the SIRAMix2 configuration for *standard* days in Dakar and Niamey we used the dust aerosol components MIAM (for the coarse mode) and MINM (for the fine mode).

3.5.3. Aerosol Characterization for *Mixture* Days

Mixture days in Dakar and Niamey were distinguishable by their moderate or high values of AOD and a marked bimodal size distribution. Table 2 shows that, for this day type, the fine mode AOD (δ_f) can be greater than the coarse optical depth (δ_c) (see 21 January). Here, the SSA does not present the signature of pure dust anymore. In contrast, it shows a lower, flat spectral signature likely due to the presence of absorbing fine particles [29]. The presence of fine aerosols is in agreement with the high value of $\alpha_{440-870}$. According to [4], mixtures of aerosol dust and biomass-burning particles were likely to happen during the selected *mixture* days due to fires at locations from the Ivory Coast to Nigeria.

This thesis is validated by the air mass back trajectories in Figure 4 (middle), which show particles in the lower layers (from 0.5 to 2 km) coming from desert areas and others in upper layers originating in the southern part of the Sahel.

Hence, for the SIRAMix2 approach, we used the aerosol components MIAM for the coarse mode and SOOT for the fine mode at both stations.

3.5.4. Aerosol Characterization for *Dusty* Days

For *dusty* days, Figures 2 and 3 show a maximum of size distribution (>1.5 $\mu m^3/\mu m^2$) with an exclusive predominance of coarse and weakly absorbing particles ($\alpha_{440–870}$ lower than 0.2 and SSA greater than 0.94, respectively), in both Dakar and Niamey. The SSA in Figures 2 and 3 shows the spectral signature typical of mineral particles, with a decrease for short wavelengths and a flat trend for longer ones. Figure 4 (right) shows that, for the *dusty* day (12 March), all particles reaching Dakar and Niamey likely originated in the Sahara desert region.

In conclusion, the SIRAMix2 approach used the aerosol components MIAM for the coarse mode and MINM for the fine mode for *dusty* days at both stations.

4. Results

In this section, we compare the different DSSF components estimated by the three methods presented in Section 3.3 against the radiation measurements taken by the ground stations in Dakar and Niamey (see Section 2.1). Surface fluxes were calculated every 10 min during the daytime according to the temporal frequency of the ground measurements used as input.

4.1. Diurnal Evolution of Surface Fluxes for Selected Dates

First, we focus on a single date for each day type. For Dakar, the dates 1 March, 23 February, 21 January, and 10 March were chosen as *clean*, *standard*, *mixture* and *dusty* days respectively. In Niamey, the selected dates were 25 November, 4 February, 11 January, and 12 March, respectively. Inputs used by the LSA-SAF, SIRAMix1, and SIRAMix2 methods are described in Section 3.4. Predominant aerosol components for each date were determined following Section 3.5 in order to run the SIRAMix2 method.

Figures 5–8 show the estimated and reference surface fluxes for the four selected dates in Dakar and Niamey. The diurnal cycle is represented on the left for diffuse DSSF, in the center for direct DSSF, and on the right for global DSSF. *In situ* measurements are plotted in black while the estimated surface fluxes are shown in blue for LSA-SAF, in green for SIRAMix1 and in red for SIRAMix2. Furthermore, the total AOD measured by AERONET is plotted in pink (see right axis). Remember that the LSA-SAF method only estimates global DSSF.

4.1.1. *Clean* Days

As can be seen in Figure 5, the aerosol load was very low in Dakar and Niamey for the *clean* days, 1 March and 25 November. Therefore, these two days were associated with a minimum of diffuse DSSF and a maximum of direct DSSF. The three global DSSF products provided similar estimated

results since aerosol effects were very weak, so their representation was not crucial. For the diffuse DSSF, the simulations slightly overestimated the *in situ* measurements, especially in Dakar (RMSE of 20.6 W/m^2 for SIRAMix1 and 14.8 W/m^2 for SIRAMix2). For direct DSSF, however, the two SIRAMix-based approaches showed similar results with a mean RMSE of about 17 W/m^2. Similar results were obtained for Niamey.

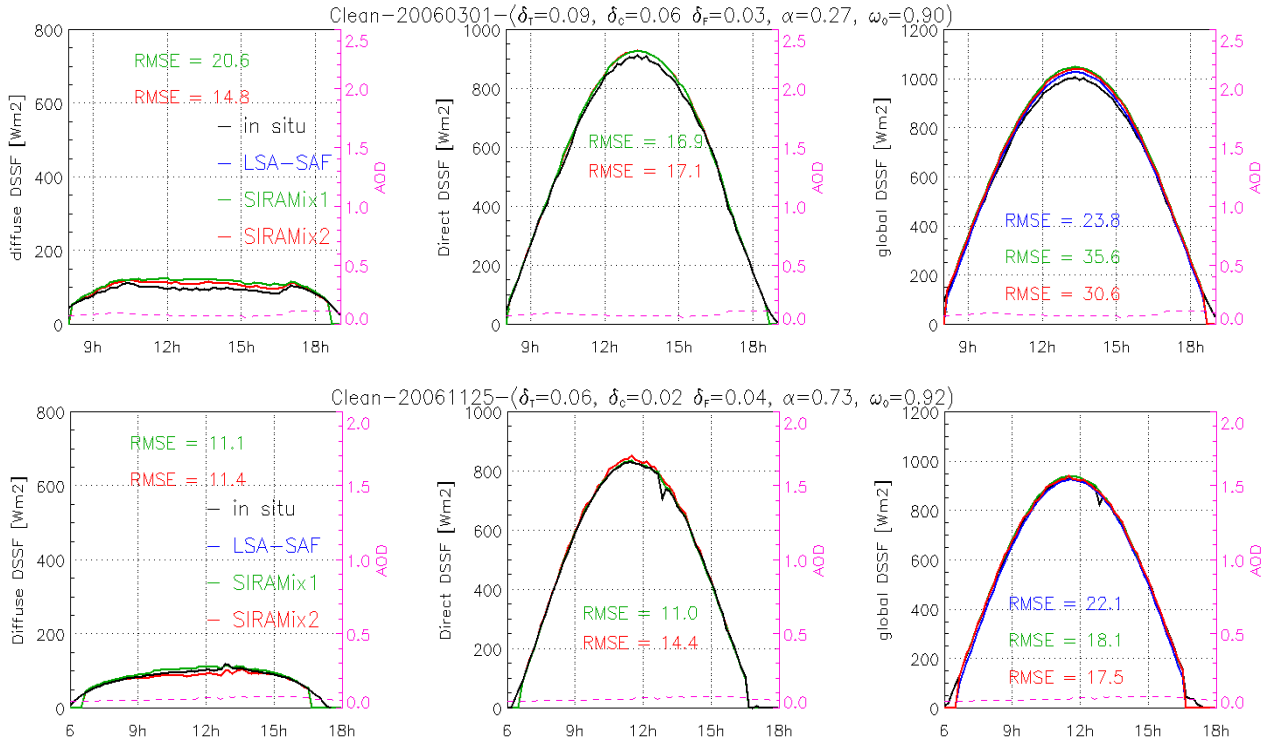

Figure 5. Diurnal cycle of diffuse, direct and global downwelling surface shortwave flux (DSSF) for *clean* days in (top) Dakar (1 March) and (bottom) Niamey (25 November). The black curve represents the *in situ* measurements, the blue is the LSA-SAF estimation, the green is the SIRAMix1 configuration simulation and the red is the simulation with the SIRAMix2 approach. The root mean square error (RMSE) between each method and the *in situ* measurement is displayed. Instantaneous aerosol optical depth (AOD) measured by the AERONET sun-photometer is shown in pink.

4.1.2. *Standard* Days

Figure 6 (top) illustrates the predominance of highly scattering coarse particles in Dakar on 15 March (coarse mode AOD of 0.35 and SSA of 0.92). The overestimation of the diffuse DSSF by SIRAMix1 (RMSE = 21 W/m^2) may point to an excess of scattering in the OPAC desert aerosol. Taking the two predominant aerosol types into account with SIRAMix2 improved the RMSE to 17.1 W/m^2. Similarly to *clean* days, direct DSSF was well simulated by the two configurations of SIRAMix. It is worth noting that the higher RMSE of the LSA-SAF product for global DSSF (77 W/m^2 against 21–22 W/m^2) was due to the underestimation of the total AOD owing to the static conditions adopted in the current LSA-SAF method. For the *standard* day chosen at Niamey—4 February represented in Figure 6 (bottom)—both SIRAMix configurations simulated the different radiation quantities with similar

accuracy. It is worth noting here that, while the two SIRAMix-based methods provide better estimations than the LSA-SAF product, is not crucial to consider aerosol composition for *standard* days because of the rather low AOD and the predominance of dust optical properties.

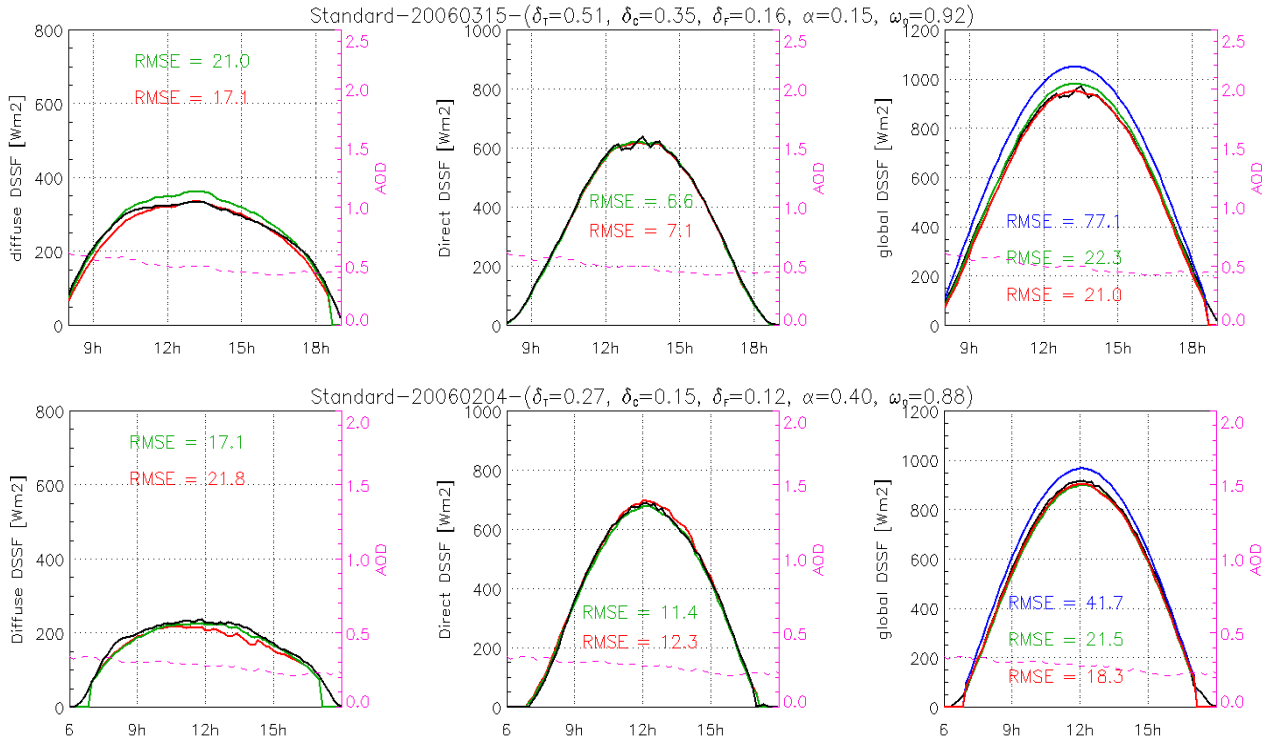

Figure 6. Same as Figure 5 for *standard* days in Dakar (15 March) and Niamey (4 February).

4.1.3. *Mixture* Days

The *mixture* day at Dakar was characterized by a predominance of fine particles from biomass burning (fine mode AOD was 0.65 while coarse AOD was 0.26) with a rather significant absorption (SSA of 0.83). Also, 11 January at Niamey was affected by a mixture of dust and biomass-burning particles (fine mode AOD was 0.26, coarse mode AOD 0.08, and SSA 0.78).

The significant improvement of the diffuse and direct DSSF estimation by SIRAMix2 is illustrated in Figure 7. First, SIRAMix1 overestimated the diffuse DSSF observations with an average RMSE of 79.1 W/m^2 in Dakar and 35.8 W/m^2 in Niamey. This was due to the inappropriateness of the desert aerosol model for this pair of dates. The fact that SIRAMix2 considered the two predominant aerosol components improved the RMSE to 29.4 W/m^2 in Dakar and to 12.2 W/m^2 in Niamey. Similar results were obtained for the direct DSSF, which improved with SIRAMix2 (RMSE decreased from 46.0 to 23.6 W/m^2 in Dakar and from 43.9 to 20.4 W/m^2 in Niamey). The RMSE obtained by LSA-SAF in terms of global DSSF (160.3 W/m^2 for Dakar and 65.6 W/m^2 for Niamey) was improved by considering the AERONET time-evolving AOD values (RMSE of 38 W/m^2 and 20 W/m^2 with SIRAMix1). When aerosol composition was taken into account with SIRAMix2, RMSE improved further for Dakar, reaching 17.4 W/m^2. The results of SIRAMix1 over Niamey must be examined with care since the moderate errors for direct DSSF (negative bias) and diffuse DSSF (positive bias) compensate each other to reach a misleading 20 W/m^2 value. The RMSE of 22.6 W/m^2 obtained with SIRAMix2 is

more significant, as the errors affecting the direct and diffuse components are much lower (20.4 and 12.2 W/m^2 for SIRAMix2 against 43.9 and 35.8 W/m^2 for SIRAMix1, respectively). The satisfactory results obtained for Niamey are noteworthy, given that the aerosol information came from the AERONET station in Banizoumbou (see Section 2.1).

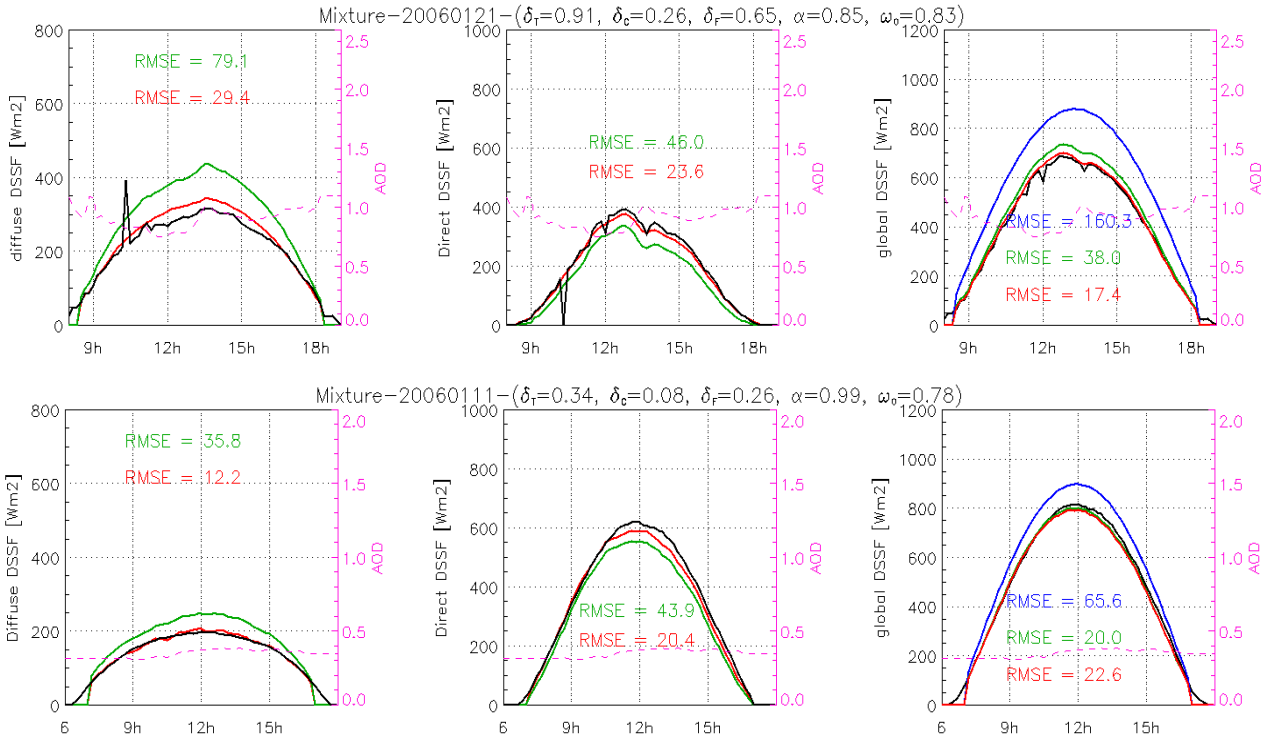

Figure 7. Same as Figure 5 for *mixture* days in Dakar (21 January) and Niamey (11 January).

4.1.4. *Dusty* Days

Figure 8 illustrates the dust event that occurred in Dakar and Niamey on 10 March. The high coarse AOD and the low Ångström coefficient for both stations point to a predominance of large aerosol particles. Also, the high SSA indicates weak absorption. These conditions led to a diffuse DSSF that was much greater than the direct DSSF. The estimation of diffuse DSSF, however, shows that the OPAC desert model used by SIRAMix1 was not appropriate, since it resulted in an underestimation of the *in situ* measurements (RMSE of 59.9 W/m^2 in Dakar and 162.6 W/m^2 in Niamey). The consideration of both fine and coarse dust particles in SIRAMix2 resulted in an RMSE for the diffuse DSSF of 29.7 W/m^2 in Dakar and 61.6 W/m^2 in Niamey. The same improvement can be observed for global DSSF, for which average RMSE was greatly improved by SIRAMix2 with respect to SIRAMix and, especially, the LSA-SAF product. The observed improvement is quite remarkable given the high aerosol load throughout the day under study (average AOD > 1.5), which generally results in large estimation errors. It is worth noting here that a small time shift can be seen between the ground and estimated surface fluxes values for Niamey, which comes from the use of aerosol data from Banizoumbou. In contrast to the *mixture* day analyzed in Section 4.1.3, the aerosol loading varied quite a lot during the day under study and therefore the 50 km between the two stations became significant. Nonetheless, the estimation of surface fluxes also improved thanks to the use of the SIRAMix-based methods and especially to SIRAMix2.

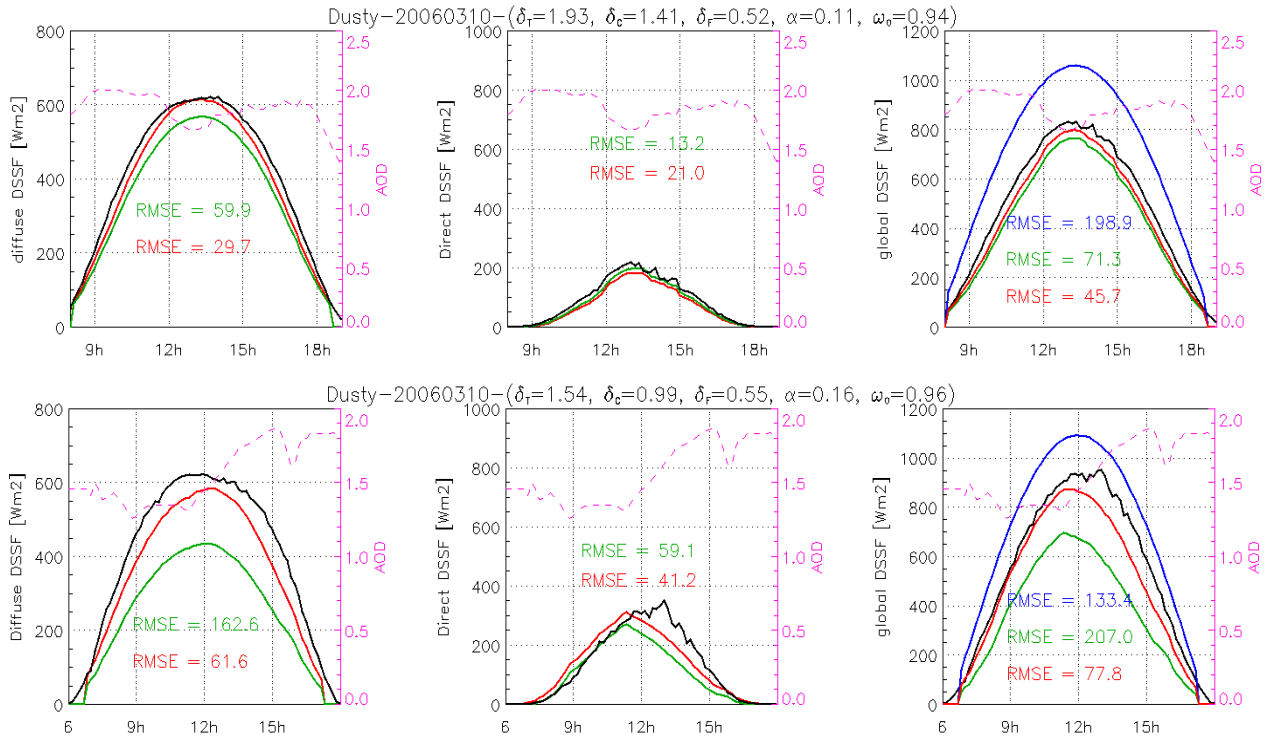

Figure 8. Same as Figure 5 for *dusty* days in Dakar (10 March) and Niamey (10 March).

4.2. Scores for All Selected Days

Table 6 summarizes the average scores considering the 20 selected clear-sky dates (see Section 2.2). The results show that the LSA-SAF global DSSF was generally improved by the fact that the two configurations of SIRAMix took the aerosol content (SIRAMix1) and the aerosol composition (SIRAMix2) into account. The average RMSE for all day types decreased from 92.7 W/m^2 for the LSA-SAF product to 42.9 W/m^2 for the SIRAMix1 configuration and 32.6 W/m^2 for SIRAMix2. The same tendency was observed in Niamey, with values of 58.8 W/m^2, 45.8 W/m^2, and 25 W/m^2, respectively. Again, scores at Niamey are significant given the use of aerosol data from Banizoumbou. The importance of considering the properties of the two predominant aerosol components with SIRAMix2 is clear. This is especially true for the estimation of the diffuse DSSF, for which SIRAMix2 always obtains the best scores. Also, the RMSE for estimated global DSSF for *dusty* days in Dakar improved from 170.2 W/m^2 for LSA-SAF to 50.7 W/m^2 for SIRAMix1, and 33.5 W/m^2 for SIRAMix2. This improvement is seen most clearly for *mixture* and *dusty* days when aerosol conditions become more challenging (*i.e.*, higher AOD values and higher probability of aerosol mixtures). In contrast, *clean* days are processed similarly by LSA-SAF and the SIRAMix-based methods due to the weakness of aerosol effects in this case. Similarly, the desert aerosol type from OPAC seems to be good enough to simulate surface fluxes for *standard* days (40% of days during the dry season).

Table 6. RMSE in W/m^2 of the global, direct and diffuse DSSF estimated by the different retrieval methods (LSA-SAF, SIRAMix1 and SIRAMix2) in Dakar and Niamey. Average values of RMSE are given per day type (*i.e.*, *clean*, *standard*, *mixture*, *dusty*) and for all selected days combined (column "All"). Bold values indicate the lowest RMSE values in each case.

DAKAR						
		Clean	***Standard***	***Mixture***	***Dusty***	**All**
Global DSSF	LSA-SAF	**24.9**	83.8	92.1	170.2	92.7
	SIRAMix1	29.3	48.8	42.8	50.7	42.9
	SIRAMix2	28.1	**37.7**	**31.2**	**33.5**	**32.6**
Direct DSSF	SIRAMix1	**15.3**	32.1	60.5	**11.2**	**29.8**
	SIRAMix2	17.5	**31.2**	**53.2**	20.6	30.6
Diffuse DSSF	SIRAMix1	22.1	36.87	79.6	45.3	45.9
	SIRAMix2	**15.8**	**25.19**	**49.4**	**32.3**	**30.7**
NIAMEY						
		Clean	***Standard***	***Mixture***	***Dusty***	**All**
Global DSSF	LSA-SAF	29.6	37.8	73.2	94.9	58.9
	SIRAMix1	21.8	28.3	21.2	111.8	45.8
	SIRAMix2	**20.0**	**28.3**	**20.2**	**34.4**	**25.7**
Direct DSSF	SIRAMix1	**10.9**	**12.6**	43.85	43.9	27.8
	SIRAMix2	15.1	13.7	**21.2**	**38.4**	**22.1**
Diffuse DSSF	SIRAMix1	16.91	22.77	29.86	131.94	50.37
	SIRAMix2	**13.10**	**21.06**	**15.16**	**51.22**	**25.13**

5. Conclusions

This study has shown the importance of considering the right aerosol composition when estimating incoming solar radiation. This was done by estimating the diurnal direct, diffuse and global DSSF corresponding to 20 dates at two stations in West Africa (Dakar and Niamey) using three different methodologies having distinct degrees of accuracy regarding aerosol representation. First, the operational LSA-SAF method, which assumes static aerosol properties, was considered. Second, two configurations of the recent surface fluxes retrieval method, referred to as SIRAMix, were used to try to improve the aerosol effects: the first (SIRAMix1) took the evolution of AOD into account with a fixed desert aerosol model and the second (SIRAMix2) accounted for variations in aerosol load and composition. SIRAMix1 reduced the bias of global DSSF by about 50% on average compared to the LSA-SAF product. However, the diffuse DSSF estimated by SIRAMix1 still contained significant errors (an average RMSE of 45.9 W/m^2 for all dates in Dakar), especially for days classified as *mixture* or *dusty*. The SIRAMix2 method, taking the optical properties of the two most predominant types (fine and coarse particles) into account, greatly improved the estimation of the diffuse radiation (average RMSE of 30.7 W/m^2 for all dates). This improvement was obtained by considering fine aerosol particles (made up of fine mineral dust, particles from biomass burning, or sea salt particles, depending on the day) that are often neglected in default desert aerosol models. Besides the better estimation of the DSSF, the improved representation of the aerosol extinction properties may be of great interest to study other radiative terms, such as radiative forcing by aerosols at the surface [14,51].

The present study may be useful for circumventing the enhanced absorption in the OPAC desert aerosol model, that has been found in some studies using aerosol observations in the Sahara desert as a reference. Most of the aerosol databases show higher absorption in the visible spectrum [52,53] than are found from *in situ* [54,55] and satellite [37] observations. These differences come from the difficulty of predicting the absorption of mineral dust because of its complex composition [43,56,57]. Also, the presence of soot particles coming from biomass burning may, in some cases, explain the higher absorption, which in turn may be compensated for by considering the two predominant aerosol types following the SIRAMix2 method.

Although this work shows the importance of considering the proper aerosol optical properties, the accurate estimation of incoming solar radiation in satellite-oriented projects such as LSA-SAF remains difficult. AERONET aerosol observations are only available at reduced spatial scales and therefore other data bases of aerosol properties at larger scale must be considered (e.g., MACC-II). Unfortunately, model-based data bases such as MACC-II are often related to decreased accuracy of the aerosol data. For instance, Ceamanos *et al.* [14] have reported biases of 76.2 and 62.0 W/m^2 for direct and diffuse DSSF using SIRAMix with MACC-II data over the North African station of Tamanrasset (with aerosol conditions similar to those at the stations studied here). These errors are much higher than those obtained by SIRAMix with AERONET aerosol load and type data in the work reported here (30.6 and 22.1 W/m^2 for direct DSSF and 30.7 and 25.1 W/m^2 for diffuse DSSF for Dakar and Niamey, respectively). The present study proves, however, that large-scale aerosol data sets might still be valuable in some cases, as has been demonstrated by the satisfactory results obtained in Niamey using the aerosol properties acquired in Banizoumbou. Another solution to be tested in the future will be the use of the improved satellite-derived aerosol products that will appear as evolutions of the current products such as MODIS [58] or MSG [59], which still need to be improved in terms of quality, temporal availability and spatial coverage.

Acknowledgments

Mamadou S. Dramé carried out this research during his stay at CRNM as a visiting scientist. Both Mamadou S. Dramé and Xavier Ceamanos were supported by EUMETSAT through the LSA-SAF project. We thank the AERONET team for the dissemination of the aerosol data. Thanks are also due to the people involved in the AMMA and ARM programs for sharing the solar radiation data. Finally, we are most grateful to Fleur Couvreux and Dominique Bouniol for sharing the cloud mask in Niamey with us.

Author Contributions

Mamadou S. Dramé and Xavier Ceamanos conceived the experimental setup, performed the experiments, analyzed the results and wrote the manuscript. Jean Louis Roujean, Aaron Boone, Jean Philippe Lafore and Dominique Carrer participated in the design of the study, the data analysis and the manuscript writing. Olivier Geoffroy contributed to the experiments.

Conflicts of Interest

The authors declare no conflict of interest.

Appendix

The bases of the SIRAMix approach are given here. For the complete physical parameterization and the corresponding references, we refer the reader to the work of Ceamanos *et al.* [14].

SIRAMix calculates the global DSSF as the sum of two irradiances

$$E = E_{dir} + E_{dif} \tag{A1}$$

where the direct DSSF (E_{dir}) is the solar irradiance coming from the direction of the Sun and the diffuse DSSF (E_{dif}) is the portion of irradiance coming from other directions due to aerosol and molecular (*i.e.*, Rayleigh) scattering.

The direct DSSF is calculated as

$$E_{dir} = E_{clean,dir} T_{aer,dir} = E_0 \nu(t) \cos\theta_0 T_{H_2O} T_{O_3} T_{mg} T_{Ray,dir} T_{aer,dir} \tag{A2}$$

where $E_{clean,dir}$ is the direct DSSF that would reach the surface of the Earth in a gaseous atmosphere free of aerosol particles. The shortwave flux at the top of atmosphere (TOA) depends on the solar constant (E_0), which is set to 1367 W·m^{-2} according to the World Meteorological Organization, the cosine of the solar zenith angle (θ_0) and the factor $\nu(t)$, which is the distance between the Sun and the Earth as a function of time. The solar flux at the TOA is then attenuated by gas absorption, which is simulated in SIRAMix through transmission functions for water vapor (T_{H2O}), ozone (T_{O3}) and uniformly mixed gases (T_{mg}). In SIRAMix, the amounts of gases are fixed for all gases except for water vapor and ozone, which constitute two inputs of the method (see Table 4). Besides the absorption of atmospheric gases, shortwave irradiance is also attenuated by Rayleigh scattering, whose transmittance reads

$$T_{Ray,dir} = \exp\left[-0.1128 m'^{0.8346} \left(0.9341 - m'^{0.9868} + 0.9391 m'\right)\right] \tag{A3}$$

where m' is the air mass corrected by the atmospheric pressure. The flux remainder at the top of the aerosol layer (TOL) is attenuated one last time before reaching the surface by aerosol particles. This is characterized by the transmittance $T_{aer,dir}$.

SIRAMix computes the diffuse DSSF as the sum of single scattering irradiance ($E_{dif,ss}$) and a multiple scattering component ($E_{dif,ss}$)

$$E_{dif} = E_{dif,ss} E_{dif,ms} \tag{A4}$$

The single scattering term is computed by multiplying the global (direct plus diffuse) flux reaching the TOL level by the diffuse aerosol transmittance

$$E_{dif,ss} = E_{clean} T_{aer,dif} = \left(E_{clean,dir} + E_{clean,dif}\right) T_{aer,dif} \tag{A5}$$

where the diffuse downwelling solar irradiance at the TOL can be expressed as

$$E_{clean,dif} = E_0 \nu(t) \cos\theta_0 T_{H_2O} T_{O_3} T_{mg} T_{Ray,dif} \tag{A6}$$

with the diffuse transmittance due to Rayleigh scattering reading

$$T_{Ray,dif} = 0.5(1 - T_{Ray,dir}) \tag{A7}$$

Using Equations (A2), (A6) and (A7) into Equation (A5), the single scattering diffuse irradiance finally reads

$$E_{dif,ss} = E_0 \nu(t) \cos\theta_0 T_{H_2O} T_{O_3} T_{mg} \left(T_{Ray,dir} + 0.5\left(1 - T_{Ray,dir}\right)\right) T_{aer,dif} \tag{A8}$$

The diffuse DSSF coming from multiple scattering is obtained as follows

$$E_{dif,ms} = \left(E_{dir} + E_{dif,ss}\right) \frac{A_{surf} A_{atm}}{1 - A_{surf} A_{atm}} \tag{A9}$$

where A_{surf} and A_{atm} are the shortwave spherical albedos of the surrounding surface and the atmosphere when illuminated from below, respectively. The albedo of the atmosphere under clear sky conditions is approximated by

$$A_{atm} \approx A_{aer} + A_{Ray} \tag{A10}$$

where A_{Ray} is set to 0.0685.

Aerosol particles in SIRAMix are characterized by the radiative quantities $T_{aer,dir}$, $T_{aer,dif}$ and A_{aer}. For SIRAMix1, the three terms are obtained from a pre-computed LUT built by the radiative transfer code libRadtran using the OPAC desert aerosol model. The LUT allows choosing the aerosol transmittance and albedo values that correspond to the actual geometrical and atmospheric conditions. For SIRAMix2, the previous aerosol quantities are calculated as the combination of the individual contributions of the two predominating aerosol modes following the model in [15]

$$\begin{aligned} T_{aer,dir} &= \frac{\delta_f}{\delta} T^f{}_{aer,dir} + \frac{\delta_c}{\delta} T^c{}_{aer,dir} \\ T_{aer,dif} &= \frac{\delta_f}{\delta} T^f{}_{aer,dif} + \frac{\delta_c}{\delta} T^c{}_{aer,dif} \\ A_{aer} &= \frac{\delta_f}{\delta} A^f{}_{aer} + \frac{\delta_c}{\delta} A^c{}_{aer} \end{aligned} \tag{A11}$$

where exponents f and c are used to distinguish aerosol quantities related to the fine aerosol mode from those corresponding to the coarse aerosol mode. The total aerosol optical depth (δ) is the sum of the fine (δ_f) and coarse (δ_c) contributions. Similar to SIRAMix1, all aerosol transmittances and albedos are calculated with libRadtran for each aerosol component in Table 3.

The formulae for the aerosol quantities complete the physical parameterization for DSSF in SIRAMix. The data inputs needed to run SIRAMix are the parameters listed in Table 4.

References

1. Marticorena, B.; Haywood, J.; Coe, H.; Formenti, P.; Liousse, C.; Mallet, M.; Pelon, J. Tropospheric aerosols over West Africa: Highlights from the AMMA international program. *Atmos. Sci. Lett.* **2011**, *12*, 19–23.

2. IPCC. Climate Change 2001: The Scientific Basis. Contribution of Working Group I to the Third Assessment Report of the Intergovernmental Panel on Climate Change. Houghton, J.T.; Ding,Y.; Griggs, D.J.; Noguer, M.; van der Linden, P.J.; Dai, X.; Maskell, K.; Johnson, C.A. Eds.; Cambridge University Press: Cambridge, United Kingdom and New York, NY, USA, p. 881.
3. Andreae, M.O.; Gelencser, A. Black carbon or brown carbon? The nature of light-absorbing carbonaceous aerosols. *Atmos. Chem. Phys.* **2006**, *6*, 3131–3148.
4. Derimian, Y.; Léon, J.-F.; Dubovik, O.; Chiapello, I.; Tanré, D.; Sinyuk, A.; Auriol, F.; Podvin, T.; Brogniez, G.; Holben, B.N. Radiative properties of aerosol mixture observed during the dry season 2006 over M'Bour, Senegal (African Monsoon Multidisciplinary Analysis campaign). *J. Geophys. Res.* **2008**, *113*, D00C09, doi:10.1029/2008JD009904.
5. Dramé, M.; Bilal, B.O.; Camara, M.; Sambou, V.; Gaye, A. Impacts of aerosols on available solar energy at Mbour, Senegal. *J. Renew. Sustain. Energy* **2012**, *4*, 013105, doi:10.1063/1.3682078.
6. Liousse, C.; Penner, J.E.; Chuang, C.; Walton, J.J.; Eddleman, H.; Cachier, H. A global three-dimensional model study of carbonaceous aerosols. *J. Geophys. Res.* **1996**, *101*, 19411–19432.
7. D'Almeida, G.A. On the variability of desert aerosol radiative characteristics. *J. Geophys. Res.* **1997**, *92*, 3017–3026.
8. Dramé, M.; Jenkins, G.; Camara, M.; Robjhon, M. Observations and Simulation of a Saharan Air Layer Event with a Mid-Tropospheric Dust Layer at Dakar, Senegal, 6–7 July 2010. *J. Geophys. Res.* **2011**, *116*, D21204, doi:10.1029/2011JD016368.
9. Trigo, I.F.; DaCamara, C.C.; Viterbo, P.; Roujean, J.L.; Olesen, F.; Barroso, C.; Camacho de Coca, F.; Carrer, D.; Freitas, S.C.; García-Haro, J.; *et al*. The Satellite Application Facility on Land Surface Analysis. *Int. J. Remote Sens.* **2011**, *32*, 2725, doi:10.1080/01431161003743199.
10. Ramier, D.; Guichard, F.; Cappelaere, B.; Kergoat, L.; Galle, S.; Timouk, F.; Boulain, N.; Boucher, M.; Taylor, C.M.; Boone, A. Impact of the monsoon on downwelling surface radiative fluxes across West Africa: An evaluation of ECMWF-IFS and satellite estimates with ground measurements. In Proceedings of EGU General Assembly 2009, Vienna, Austria, 19–24 April 2009.
11. Kocha, C.; Lafore, J.-P.; Tulet, P. High resolution simulation of a major West African dust storm: Comparison with observations and impact of dusts. *Q. J. R. Meteorol. Soc.* **2012**, *138*, 455–470, doi:10.1002/qj.927.
12. Kocha, C.; Tulet, P.; Lafore, J.-P.; Flamant, C. The importance of the diurnal cycle of Aerosol Optical Depth in West Africa. *Geophys. Res. Lett.*, **2013**, *40*, 785–790, doi:10.1002/grl.50143.
13. Redelsperger, J.-L.; Thorncroft, C.D.; Diedhiou, A.; Lebel, T.; Parker, D.J.; Polcher, J. African Monsoon Multidisciplinary Analysis: An International Research Project and Field Campaign. *Bull. Am. Meteorol. Soc.* **2006**, *87*, 1739–1746.
14. Ceamanos, X.; Carrer, D.; Roujean, J.-L. Improved retrieval of direct and diffuse downwelling surface shortwave flux in cloudless atmosphere using dynamic estimates of aerosol content and type: Application to the LSA-SAF project. *Atmos. Chem. Phys.* **2014**, *14*, 8209–8232, doi:10.5194/acp-14-8209-2014.
15. Ceamanos, X.; Carrer, D.; Roujean, J.-L. An efficient approach to estimate the transmittance and reflectance of a mixture of aerosol components. *Atmos. Res.* **2014**, *137*, 125–135, doi:10.1016/j.atmosres.2013.09.009.

16. Morcrette, J.-J.; Boucher, O.; Jones, L.; Salmond, D.; Bechtold, P.; Beljaars, A.; Benedetti, A.; Bonet, A.; Kaiser, J.W.; Razinger, M.; *et al*. Aerosol analysis and forecast in the European Centre for Medium-Range Weather Forecasts Integrated Forecast System: Forward modeling. *J. Geophys. Res.* **2009**, *114*, D06206, doi:10.1029/2008JD011235.
17. Chiapello, I.; Bergametti, G.; Gomes, L.; Chatenet, B.; Duac, F.; Pimenta, J.; Suares, E.S. An additional low layer transport of Sahelien and Saharan dust over the north-eastern tropical Atlantic. *Geophys. Res. Lett.* **1995**, *22*, 3191–3194.
18. Fomba, K.W.; Müller, K.; van Pinxteren, D.; Poulain, L.; van Pinxteren, M.; Herrmann, H. Long-term chemical characterization of tropical and marine aerosols at the CVAO: Field studies (2007 to 2011). *Atmos. Chem. Phys. Discuss.* **2014**, *14*, 3917–3971, doi:10.5194/acpd-14-3917-2014.
19. Heinold, B.; Tegen, I.; Schepanski, K.; Tesche, M.; Esselborn, M.; Freudenthaler, V.; Gross, S.; Kandler, K.; Knippertz, P.; Müller, D.; *et al*. Regional modelling of Saharan dust and biomass burning smoke—Part 1: Model description and evaluation. *Tellus B* **2011**, *63*, 781–799.
20. Müller, T.; Henzing, J.S.; de Leeuw, G.; Wiedensohler, A.; Alastuey, A.; Angelov, H.; Bizjak, M.; Collaud Coen, M.; Engström, J.E.; Gruening, C.; *et al*. Characterization and intercomparison of aerosol absorption photometers: Result of two intercomparison workshops. *Atmos. Meas. Tech.* **2011**, *4*, 245–268.
21. Holben, B.N.; Eck, T.F.; Slutsker, I.; Tanré, D.; Buis, J.P.; Setzer, A.; Vermote, E.; Reagan, J.A.; Kaufman, Y.J.; Nakajima, T. AERONET-A federated instrument network and data archive for aerosol characterization. *Remote Sens. Environ.* **1998**, *66*, 1–16, doi:10.1016/S0034-4257(98)00031-5.
22. Dubovik, O.; King, M.D. A flexible inversion algorithm for retrieval of aerosol optical properties from sun and sky radiance measurements. *J. Geophys. Res.* **2000**, *105*, 20673–20696.
23. Ackerman, P.; Stokes, G. The atmospheric Radiation Measurement Program. *Phys. Today* **2003**, *56*, 38–44.
24. Lebel, T.; Parker, D.J.; Flamant, C.; Bourles, B.; Marticorena, M.; Mougin, E.; Peugeot, C.; Diedhiou, A.; Haywood, J.M.; Ngamini, J. The AMMA field campaigns: Multiscale and multidisciplinary observations in the West African region. *QJRMS* **2009**, *136*, 8–33, doi:10.1002/qj.486.
25. Milton, S.F.; Greed, G.; Brooks, M.E.; Haywood, J.; Johnson, B.; Allan, R.P.; Grey, W.M.F. Modelled and observed atmospheric radiation balance during West Africa dry season: Role of mineral dust, biomass burning aerosol; surface albedo. *J. Geophys. Res.* **2008**, *113*, D00C02, doi:10.1029/2007JD009741.
26. Bouniol, D.; Couvreux, F.; Kamsu-Tamo, P.-H.; Leplay, M.; Guichard, F.; Favot, F.; O'Connor, E.J. Diurnal and Seasonal Cycles of Cloud Occurrences, Types, and Radiative Impact over West Africa. *J. Appl. Meteorol. Climatol.* **2012**, *51*, 534–553.
27. Ångström, A. The parameters of atmospheric turbidity. *Tellus* **1964**, *16*, 64–75.
28. Fouquart, Y.; Bonnel, B.; Roquai, M.C.; Santer, R.; Cerf, A. Observations of Saharan aerosols: Results of ECLATS field experiment: Optical thicknesses and aerosol size distribution. *J. Clim. Appl. Meteorol*. **1987**, *26*, 28–37.
29. Dubovik, O.; Holben, B.; Eck, T.F.; Smirnov, A.; Kaufman, Y.J.; King, M.D.; Tanré, D.; Slutsker, I. Variability of absorption and optical properties of key aerosol types observed in worldwide locations. *J. Atmos. Sci.* **2002**, *59*, 590–608.

30. Shettle, E.P. Fenn, R.W. *Models for the Aerosols of the Lower Atmosphere and the Effects of Humidity Variations of Their Optical Properties*; AFGL-TR-790214; Air Force Geophysics Laboratory: Hanscom AFB, MA, USA, 1979.
31. WMO. *Radiation Commission of IAMAP Meeting of Experts on Aerosol and Their Climatic Effects*; WCP55; World Meteorological Organization: Williamsburg, VA, USA, 1983; pp. 28–30.
32. Koepke, P.; Hess, M.; Schult, I.; Shettle, E.P. *Global Aerosol Data Set*; Report No. 243; Max-Planck-Institut für Meteorologie: Hamburg, Germany, 1997; p. 44.
33. Hess, M.; Koepke, P.; Schult, I. Optical Properties of Aerosols and Clouds: The Software Package OPAC. *Bull. Am. Meteorol. Soc.* **1998**, *79*, 831–844.
34. Tanré, D.; Kaufman,Y.J.; Holben, B.N.; Chatenet, B.; Karnieli, A.; Lavenu, F.; Blarel, L.; Dubovik, O.; Remer, L.A.; Smirnov, A. Climatology of dust aerosol size distribution and optical properties derived from remotely sensed data in the solar spectrum. *J. Geophys. Res.* **2001**, *106*, 18205–18217.
35. Kim, J.; Gu, Y.; Liou, K.N. The Impact of Direct Aerosol Radiative Forcing on Surface Insolation and Spring Snowmelt in the Southern Sierra Nevada. *J. Hydrometeorol.* **2006**, *7*, 976–983.
36. Mayer, B.; Kylling, A. Technical note: The LibRadtran software package for radiative transfer calculations—Description and examples of use. *Atmos. Chem. Phys.* **2005**, *5*, 1855–1877, doi:10.5194/acp-5-1855-2005.
37. Kaufman, Y.J.; Tanré, D.; Dubovik, O.; Karnieli, A.; Remer, L.A. Absorption of sunlight by dust as inferred from satellite and ground-based remote sensing. *Geophys. Res. Lett.* **2001**, *28*, 1479–1482.
38. Colarco, P.R.; Toon, O.B.; Torres, O.; Rasch, P.J. Determining the UV imaginary part of refractive index of Saharan dust particles from TOMS data and a three dimensional model of dust transport. *J. Geophys. Res.* **2002**, *107*, 4289, doi:10.1029/2001JD000903.
39. Haywood, J.M.; Allan, R.P.; Culverwell, I.; Slingo, A.; Milton, S.; Edwards, J.; Clerbaux, N. Can desert dust explain the outgoing longwave radiation anomaly over the Sahara during July 2003? *J. Geophys. Res.* **2005**, *110*, D05105, doi:10.1029/2004JD005232.
40. Petzold, A.; Rasp, K.; Weinzierl, B.; Esselborn, M.; Hamburger, T.; Durnbrack, A.; Kandler, K.; Schutz, L.; Knippertz, P.; Fiebig, M.; Virkkula, A. Saharan dust refractive index and optical properties from aircraft-based observations during SAMUM 2006. *Tellus B* **2009**, *61*, 118–130.
41. McConnell, C.L.; Formenti, P.; Highwood, E.J.; Harrison, M.A.J. Using aircraft measurements to determine the refractive index of Saharan dust during the DODO Experiments. *Atmos. Chem. Phys.* **2010**, *10*, 3081–3098, doi:10.5194/acp-10-3081-2010.
42. Ackerman, P.; Toon, O.B. Absorption of visible radiation in atmosphere containing mixtures of absorbing and nonabsorbing particles. *Appl. Opt.* **1981**, *20*, 3661–3668.
43. Martins, J.V.; Artaxo, P.; Liousse, C.; Reid, J.S.; Hobbs, P.V.; Kaufman, Y.J. Effects of black carbon content, particle size, and mixing on light absorption by aerosol from biomass burning in Brazil. *J. Geophys. Res.* **1998**, *103*, 32041–32050.
44. Geiger, B.; Meurey, C.; Lajas, D.; Franchistéguy, L.; Carrer, D.; Roujean, J.-L. Near real-time provision of downwelling short-wave radiation estimates derived from satellite observations. *Meteorol. Appl.* **2008**, *15*, 411–420, doi:10.1002/met.84.

45. Remer, L.A.; Kaufman, Y.J. Dynamic aerosol model: Urban/industrial aerosol. *J. Geophys. Res.* **1998**, *103*, 13859–13871.
46. Ginoux, P. Effects of nonsphericity on mineral dust modeling. J. Geophys. Res. **2003**, 108, 4052, doi:10.1029/2002JD002516.
47. Geiger, B.; Carrer, D.; Franchistéguy, L.; Roujean, J.L.; Meurey, C. Land surface albedo derived on a daily basis from Meteosat Second Generation observations. *IEEE Trans. Geosci. Remote. Sens.* **2008**, *46*, 3841–3856, doi:10.1109/TGRS.2008.2001798.
48. Draxler, R.R.; et Hess, G.D. An overview of the HYSPLIT-4 modelling system for trajectories, dispersion and deposition. *Aust. Meteorol. Mag.* **1998**, *47*, 295–308.
49. Léon, J.F.; Derimian, Y.; Chiapello, I.; Tanré, D.; Podvin, T.; Chatenet, B.; Diallo, A.; Deroo, C. Aerosol vertical distribution and optical properties over Mbour (16.96°W, 14.39°N), Senegal from 2000 to 2008. *Atmos. Chem. Phys.* **2009**, *9*, 9249–9261.
50. Semou, N. Etude de la Variabilité des Flux D'humidité sur Dakar en Période Pré-Installation de la Mousson. Master's Thesis, École Supérieure Polytechnique, Université Cheikh Anta Diop de Dakar, Dakar, Sénégal, 2012; p. 50.
51. Xu, H.; Ceamanos, X.; Roujean, J.-L.; Carrer, D.; Xue, Y. Can satellite-derived aerosol optical depth quantify the surface aerosol radiative forcing? *Atmos. Res.* **2014**, *150*, 151–167.
52. Patterson, E.M.; Gillete, D.A.; Stockton, B.H. Complex index of refraction between 300 and 700 nm for Saharan aerosol. *J. Geophys. Res.* **1977**, *82*, 3153–3160.
53. Haywood, J.M.; Francis, P.N.; Geogdzhayev, I.; Mishchenko, M.; Frey, R. Comparison of Saharan dust aerosol optical depth retrieved using aircraft mounted pyranometers and 2-channel AVHRR algorithms. *Geophys. Res. Lett.* **2001**, *28*, 2393–2396, doi:10.1029/2000GL012625.
54. Fouquart, Y.; Brogniez, C.; Buriez, L.; Smith, L.; Morcrette, J.J. Observations of Saharan aerosols: Results of ECLATS Field experiment. Part II: Broadband radiative characteristics of the aerosols and vertical radiative flux divergence. *J. Clim. Appl. Meteorol.* **1987**, *26*, 38–52.
55. Otterman, J.; Fraser, R.S.; Bahethi, O.P. Characterization of tropospheric desert aerosols at solar wavelengths by multispectral radiometry from Landsat. *J. Geophys. Res.* **1982**, *87*, 1270–1278.
56. Claquin, T.; Schulz, M.; Balkanski, Y.; Boucher, O. Uncertainties in assessing radiative forcing by mineral dust. *Tellus* **1998**, *50*, 491–505.
57. Sokolik, I.N.; Toon, O.B. Incorporation of mineralogical composition into models of the radiative properties of mineral aerosol from UV to IR wavelengths. *J. Geophys. Res.* **1999**, *104*, 9423–9444.
58. Remer, L.A.; Kaufman, Y.J.; Tanré, D.; Mattoo, S.; Chu, D.A.; Martins, J.V.; Li, R.-R.; Ichoku, C.; Levy, R.C.; Kleidman, R.G.; *et al*. The MODIS aerosol algorithm, products, and validation. *J. Atmos. Sci.* **2005**, *62*, 947–973, doi:10.1175/JAS3385.1.
59. Carrer, D.; Ceamanos, X.; Six, B.; Roujean, J.-L. AERUS-GEO: A newly available satellite-derived aerosol optical depth product over Europe and Africa. *Geophys. Res. Lett.* **2014**, *41*, doi:10.1002/2014GL061707.